

## Computational Studies of the Relative Rates for Migratory Insertions of Alkenes into Square-Planar, Methyl-, Amido-, and Hydroxo Complexes of Rhodium

Jesse W. Tye and John F. Hartwig\*

Department of Chemistry, University of Illinois Urbana-Champaign, 600 South Mathews Avenue, Box 58-6, Urbana, Illinois 61801

Received March 12, 2009; E-mail: jhartwig@illinois.edu

**Abstract:** The relative rates of the migratory insertions of alkenes into the M–X bonds of  $(\text{PMe}_3)_2\text{Rh}(\eta^2\text{-CH}_2=\text{CHR})(\text{X})$  (R = H, Me; X =  $\text{CH}_3$ ,  $\text{NH}_2$ , OH) have been analyzed by DFT calculations. These insertions are computed to form metallacycles containing a metal–carbon bond and either an agostic interaction, a dative metal–nitrogen bond, or a dative metal–oxygen bond. The computed barriers for migratory insertion into the metal–hydroxo and metal–amido bonds are lower than those for insertion into the metal–methyl bond. Application of Bader’s atoms-in-molecules analysis and natural localized molecular orbital analysis implies that the barriers for alkene insertion into M–X bonds are controlled by the degree of M–X bonding in the transition state, which correlates with the degree of M–X bonding in the initial product. The Rh–X bond orders in the transition states for migratory insertion of ethylene into the Rh– $\text{NH}_2$  and Rh–OH bonds in  $(\text{PH}_3)_2\text{Rh}(\eta^2\text{-C}_2\text{H}_4)(\text{NH}_2)$  and  $(\text{PH}_3)_2\text{Rh}(\eta^2\text{-C}_2\text{H}_4)(\text{OH})$  are much larger than that in the transition state for insertion into the Rh–C bond of  $(\text{PH}_3)_2\text{Rh}(\eta^2\text{-C}_2\text{H}_4)(\text{CH}_3)$ . The free energy barriers for 1,2- and 2,1-insertions of propene into the rhodium complexes were also calculated, and the barrier for 1,2-insertion was found to be lower than that for 2,1-insertion. Most striking, the  $\Delta\Delta G^\ddagger$  values for 1,2- versus 2,1-insertion of propene into these rhodium complexes were calculated to increase in the order X =  $\text{CH}_3 < \text{NH}_2 < \text{OH}$ . The increasing stability of the 1,2-insertion product with increasing polarity of the C–X bonds parallels the relative stabilities of linear versus branched alkanes, amines, and alcohols.

### Introduction

Migratory insertion is a fundamental class of reaction in organotransition metal chemistry.<sup>1–3</sup> Migratory insertions of alkenes into metal–carbon bonds are elementary reactions in diverse catalytic processes that include many types of polymerizations of alkenes,<sup>4–7</sup> difunctionalizations of alkenes that form carbon–carbon bonds,<sup>8–12</sup> hydroarylations of alkenes,<sup>13–18</sup> as well as olefinations of aryl halides commonly called the

Mizoroki–Heck reaction.<sup>19–22</sup> The migratory insertion of an alkene into a metal–heteroatom bond is less common but has been proposed to occur during carboaminations of alkenes,<sup>23–26</sup> hydroaminations,<sup>27,28</sup> and oxidative aminations of olefins,<sup>29</sup> and strong evidence has been provided for the intermediacy of this reaction during Wacker oxidations under conditions of low halide to produce aldehydes, ketones, and vinyl ethers.<sup>30–35</sup> The

- Hartwig, J. F. *Organotransition Metal Chemistry*; University Science Books: Sausalito, CA, in press.
- Crabtree, R. H. *The Organometallic Chemistry of the Transition Metals*, 5th ed.; Wiley: New York, 2009.
- Collman, J. P.; Hegedus, L. S.; Norton, J. R.; Finke, R. G. *Principles and Applications of Organotransition Metal Chemistry*; University Science Books: Mill Valley, CA, 1987.
- Ittel, S. D.; Johnson, L. K.; Brookhart, M. *Chem. Rev.* **2000**, *100*, 1169.
- Mecking, S. *Angew. Chem., Int. Ed.* **2001**, *40*, 534.
- Gibson, V. C.; Spitzmesser, S. K. *Chem. Rev.* **2003**, *103*, 283.
- Grubbs, R. H.; Coates, G. W. *Acc. Chem. Res.* **1996**, *29*, 85.
- Nakao, Y.; Idei, H.; Kanyiva, K. S.; Hiyama, T. *J. Am. Chem. Soc.* **2009**, *131*, 5070.
- Nakao, Y.; Hirata, Y.; Hiyama, T. *J. Am. Chem. Soc.* **2006**, *128*, 7420.
- Hirata, Y.; Inui, T.; Nakao, Y.; Hiyama, T. *J. Am. Chem. Soc.* **2009**, *131*, 6624.
- Nakao, Y.; Ebata, S.; Yada, A.; Hiyama, T.; Ikawa, M.; Ogoshi, S. *J. Am. Chem. Soc.* **2008**, *130*, 12874.
- Watson, M. P.; Jacobsen, E. N. *J. Am. Chem. Soc.* **2008**, *130*, 12594.
- Periana, R. A.; Liu, X. Y.; Bhalla, G. *Chem. Commun.* **2002**, 3000.
- Oxgaard, J.; Periana, R. A.; Goddard, W. A., III. *J. Am. Chem. Soc.* **2004**, *126*, 11658.
- Lail, M.; Bell, C. M.; Conner, D.; Cundari, T. R.; Gunnoe, T. B.; Petersen, J. L. *Organometallics* **2004**, *23*, 5007.
- Tan, K. L.; Bergman, R. G.; Ellman, J. A. *J. Am. Chem. Soc.* **2002**, *124*, 13964.
- Thalji, R. K.; Ahrendt, K. A.; Bergman, R. G.; Ellman, J. A. *J. Am. Chem. Soc.* **2001**, *123*, 9692.
- Murai, S.; Kakiuchi, F.; Sekine, S.; Tanaka, M.; Kamatani, A.; Motohiro, S.; Chanti, N. *Nature* **1993**, *366*, 529.
- Amatore, C.; Jutand, A. *Acc. Chem. Res.* **2000**, *33*, 314.
- Beletskaya, I. P.; Cheprakov, A. V. *Chem. Rev.* **2000**, *100*, 3009.
- Heck, R. F. *Acc. Chem. Res.* **1969**, *2*, 10.
- Heck, R. F. *Acc. Chem. Res.* **1979**, *12*, 146.
- Nakha, J. S.; Kampf, J. W.; Wolfe, J. P. *J. Am. Chem. Soc.* **2006**, *128*, 2893.
- Ney, J. E.; Wolfe, J. P. *Angew. Chem. Int. Ed.* **2004**, *43*, 3605.
- Ney, J. E.; Wolfe, J. P. *J. Am. Chem. Soc.* **2005**, *127*, 8644.
- Wolfe, J. P. *Eur. J. Org. Chem.* **2007**, 571, 2007.
- Casalnuovo, A. L.; Calabrese, J. C.; Milstein, D. *J. Am. Chem. Soc.* **1988**, *110*, 6738.
- Zhou, J.; Hartwig, J. F. *J. Am. Chem. Soc.* **2008**, *130*, 12220.
- Liu, G. S.; Stahl, S. S. *J. Am. Chem. Soc.* **2007**, *129*, 6328.
- El-Qisairi, A. K.; Qaseer, H. A.; Henry, P. M. *J. Organomet. Chem.* **2002**, *656*, 168.
- Gragor, N.; Henry, P. M. *J. Am. Chem. Soc.* **1981**, *103*, 681.
- Hamed, O.; Henry, P. M. *Organometallics* **1997**, *16*, 4903.

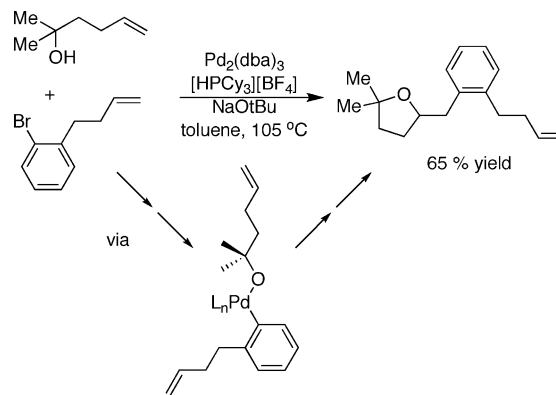
migratory insertion of alkenes into M–N bonds has most recently been used to generate polymers containing terminal amino groups.<sup>36</sup>

Despite the importance of migratory insertions into metal–carbon, –nitrogen, and –oxygen bonds, few studies allow one to compare the mechanism, rate, and selectivity for insertions of olefins into these three classes of metal–ligand bonds. Until most recently, insertions of olefins into the metal–oxygen and –nitrogen bonds of discrete metal–alkoxo and –amido complexes were limited to the insertions of polarized or strained alkenes and the intramolecular insertions of alkenes into lanthanide–alkyl complexes. In two cases, insertions of electronically activated alkenes occurred into the metal–nitrogen and metal–oxygen bond over the metal–carbon or metal–hydrogen bond, but this preference could be attributed to the electron-poor<sup>37,38</sup> or polarized<sup>39,40</sup> property of the alkene. In a third case, reaction of the strained olefin norbornene with an Ir(III) amide hydride complex formed the product from migratory insertion into the metal–nitrogen bond over the metal–hydride bond.<sup>41</sup>

Other experimental data pertains to insertions of alkenes into lanthanide–amido bonds. Marks reported the migratory insertions of pendant alkenes into lanthanide amides. In particular, the amido, amine complex  $[\text{Cp}^*_2\text{Ln}(\text{NH}(\text{CH}_2)_3\text{CH}=\text{CH}_2)(\text{NH}_2(\text{CH}_2)_3\text{CH}=\text{CH}_2)]$  was shown to insert the pendant alkene into the Ln–N bond to yield the five-membered azacycle 2-methylpyrrolidine.<sup>42</sup> Although Marks' studies did not allow a direct comparison of the rates of insertion of alkenes into lanthanide–amide and –alkyl bonds, studies of reactions catalyzed by lananocene complexes imply that insertion into a lanthanide–amide bond is slower than insertion into a lanthanide–alkyl bond.<sup>42,43</sup> The rate of alkene polymerization catalyzed by this type of lanthanide complex is much faster than the rate of alkene hydroamination catalyzed by related complexes.<sup>44</sup>

Although few isolated, late transition-metal complexes insert unactivated alkenes into metal–amide and –alkoxo bonds, a few studies of catalytic reactions suggest that the migratory insertion of alkenes into  $d^8$  transition-metal–amido and –alkoxo bonds can be more facile than the migratory insertion of alkenes into  $d^8$  transition-metal–alkyl bonds. The products of palladium-catalyzed carboetherification and carboamination reactions of  $\gamma$ -hydroxy- and  $\gamma$ -aminoalkenes have been shown by Wolfe and co-workers to yield products that are consistent with faster insertion of alkenes into palladium–amido and –alkoxo bonds than into palladium–aryl bonds.<sup>23–26</sup> In one particularly revealing example (Scheme 1), the palladium-catalyzed reaction of an aryl bromide that contained a tethered alkene with a  $\gamma$ -hydroxyalkene yielded the 2-arylmethyl tetrahydrofuran re-

Scheme 1



sulting from insertion of the alkene into the metal–alkoxide bond instead of the metal–aryl bond.

Finally, the authors' laboratory reported rare examples of discrete transition-metal–amido and –alkoxo complexes that undergo insertions of unactivated alkenes into the metal–amide and metal–alkoxo bonds. Kinetic and stereochemical studies were consistent with a mechanism in which migratory insertion of the alkene into the Rh–N or Rh–O bonds occurred within complexes of the type  $(\text{PEt}_3)_2\text{Rh}(\eta^2\text{-alkene})(\text{XR})$  ( $\text{X} = \text{NH}, \text{O}$ ).<sup>45,46</sup> These insertions of alkenes into rhodium–alkoxo and –amido complexes appeared to be faster than insertions into rhodium–alkyl complexes and to occur with regioselectivity that contrasts that of insertions of alkenes and vinylarenes into metal–alkyl and –aryl bonds.<sup>47</sup>

Thus, scattered data have been gained on the relative rates for migratory insertions of alkenes into metal–carbon, –nitrogen, and –oxygen bonds, but studies that reveal the factors that control the relative rates of these migratory insertions and the regioselectivity of the insertion of unsymmetrical alkenes into these bonds has been lacking. The regioselectivity for migratory insertions of alkenes into metal–carbon bonds is known to depend on the electronic properties of the substituent attached to the alkene, but the effects of the anionic ligand (methyl, amide, or hydroxide) involved in the insertion process are unknown. The insertion of propene into metal–alkyl bonds has been shown to form products from 1,2-insertion, 2,1-insertion, or both (eq 1),<sup>48</sup> but catalytic reactions of alkenes that have been proposed to occur by insertions of alkenes into metal–nitrogen and metal–oxygen bonds have always formed products that would result from 1,2-insertion.<sup>29–35,46,49</sup> Thus, the barriers for 2,1-insertions into amides and alkoxides that would lead to products containing amino or alkoxo functionality at the terminal carbon are unknown.

For this reason, we used computational methods to assess the relative energetics for insertions of alkenes into amido and alkoxo complexes of a late transition metal, the transition-state energies for 1,2- and 2,1-insertions of alkenes into these complexes (eq 1), and the factors that control these relative

(33) Hamed, O.; Thompson, C.; Henry, P. M. *J. Org. Chem.* **1997**, *62*, 7082.

(34) Henry, P. M.; Ward, G. A. *J. Am. Chem. Soc.* **1971**, *93*, 1494.

(35) Wan, W. K.; Zaw, K.; Henry, P. M. *J. Mol. Catal.* **1982**, *16*, 81.

(36) Amin, S. B.; Marks, T. J. *J. Am. Chem. Soc.* **2007**, *129*, 10102.

(37) Bryndza, H. E. *Organometallics* **1985**, *4*, 406.

(38) Bryndza, H. E.; Calabrese, J. C.; Wreford, S. S. *Organometallics* **1984**, *3*, 1603.

(39) Cowan, R. L.; Trogler, W. C. *Organometallics* **1987**, *6*, 2451.

(40) Cowan, R. L.; Trogler, W. C. *J. Am. Chem. Soc.* **1989**, *111*, 4750.

(41) Casalnuovo, A. L.; Calabrese, J. C.; Milstein, D. *J. Am. Chem. Soc.* **1988**, *110*, 6738.

(42) Gagne, M. R.; Stern, C. L.; Marks, T. J. *J. Am. Chem. Soc.* **1992**, *114*, 275.

(43) Gagne, M. R.; Marks, T. J. *J. Am. Chem. Soc.* **1989**, *111*, 4108.

(44) Jeske, G.; Lauke, H.; Mauermann, H.; Swepston, P. N.; Schumann, H.; Marks, T. J. *J. Am. Chem. Soc.* **1985**, *107*, 8091.

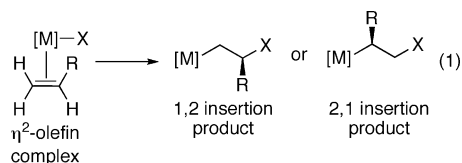
(45) Zhao, P.; Krug, C.; Hartwig, J. F. *J. Am. Chem. Soc.* **2005**, *127*, 12066.

(46) Zhao, P.; Incarvito, C. D.; Hartwig, J. F. *J. Am. Chem. Soc.* **2006**, *128*, 9642.

(47) Under reaction conditions similar to those of the reactions of propene and styrene with  $\text{PEt}_3$ -ligated rhodium–alkoxo and –amido complexes,  $(\text{PEt}_3)_3\text{RhMe}$  does not form products from insertion of propene or styrene.

(48) Svejda, S. A.; Brookhart, M. *Organometallics* **1999**, *18*, 65.

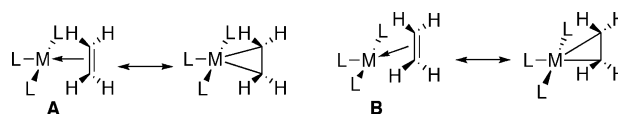
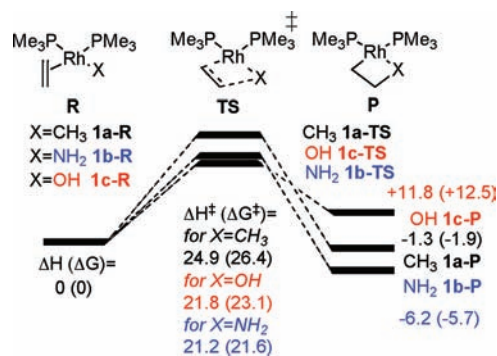
(49) Zhao, P.; Hartwig, J. F. *Organometallics* **2008**, *27*, 4749.



energies. A few computational studies have been conducted on the insertions of alkenes into metal–amido complexes, but these studies have focused exclusively on migratory insertions into electrophilic lanthanide–amide complexes.<sup>50–57</sup> Computational studies of the migratory insertion of alkenes into late transition-metal–amide and –alkoxide bonds that would allow a comparison to the many studies on the insertions of alkenes into late metal–alkyl complexes<sup>58–65</sup> have not been published. The most relevant prior study was conducted with extended Hückel theory prior to the development of modern DFT methods. These calculations led to the conclusion that migratory insertions of alkenes into metal–hydroxo bonds would be unfeasible if controlled by frontier orbitals,<sup>61</sup> this assertion is clearly inconsistent with recent experimental results.

Here, we report a computational study of the insertion of ethylene and propene into square-planar rhodium–methyl, –amido, and –hydroxo complexes using density functional theory.<sup>66</sup> These calculations have been conducted on the 16-electron, rhodium  $\eta^2$ -alkene complexes  $(\text{PMe}_3)_2\text{Rh}(\eta^2\text{-CH}_2\text{=CHR})(\text{X})$  ( $\text{R} = \text{H, Me; X} = \text{CH}_3, \text{NH}_2, \text{OH}$ ), which are closely related to the species deduced from kinetic studies to be intermediates in our recently reported insertions of alkenes into the metal–nitrogen and metal–oxygen bonds of rhodium–amido and –alkoxo complexes.<sup>46,49</sup> These studies show that the computed free energy barriers for migratory insertions of alkenes into these amido and –hydroxo complexes of a late transition metal are lower than those for migratory insertions into the analogous methyl complex, that the origin of the low barriers for these insertions into the metal–heteroatom bonds results from a smaller degree of bond cleavage in the transition state, due to the presence of dative bonds between the heteroatoms and the metal centers in the transition states and that the difference in transition-state energies for 1,2- and 2,1-insertion

Scheme 2

Figure 1. Two potential structures for  $d^8$  alkene complexes.

of propene increases with the electronegativity of the metal-bound atom.

## Results and Discussion

Computational studies of the insertion of ethylene into rhodium–amide, –alkoxo, and –alkyl complexes and the insertion of propene into the same set of complexes have been conducted. These studies were carried out using density functional theory with the B3LYP functional as implemented in the Gaussian 03 software with polarized triple- $\zeta$  basis sets. The use of the B3LYP density functional with polarized double- $\zeta$  and/or larger basis sets have been shown to yield accurate results for many rhodium systems.<sup>67–71</sup>

**Computed Barriers for Ethylene Insertion Into the Rh–X Bonds of  $(\text{PMe}_3)_2\text{Rh}(\eta^2\text{-C}_2\text{H}_4)(\text{X})$  ( $\text{X} = \text{CH}_3, \text{NH}_2, \text{OH}$ ).** Scheme 2 shows the reactant, transition-state, and product structures, computed enthalpies, and computed free energies for the migratory insertion of ethylene into the rhodium–amide, –hydroxo, and –methyl complexes  $(\text{PMe}_3)_2\text{Rh}(\eta^2\text{-C}_2\text{H}_4)(\text{X})$  ( $\text{X} = \text{CH}_3, \text{NH}_2, \text{OH}$ ). The energy-minimized structures of the alkene-ligated starting complexes are noteworthy. A survey of the Cambridge Structural Database shows that most alkene complexes of  $d^8$  transition metals have a structure in which the centroid of the C–C double bond lies in the square plane defined by the other ligands (represented by structure **A** shown in Figure 1). However, a few such rhodium complexes have a structure (represented by structure **B** in Figure 1) in which the centroid of the C–C double bond of the alkene lies out of the square plane defined by the other ligands.<sup>72,73</sup> The geometry-optimized structures of the starting neutral alkene rhodium complexes in

- (50) Hunt, P. A. *Dalton Trans.* **2007**, 1743.  
 (51) Kieken, E.; Wiest, O.; Helquist, P.; Cucciolito, M. E.; Flores, G.; Vitagliano, A.; Norrby, P.-O. *Organometallics* **2005**, *24*, 3737.  
 (52) Motta, A.; Fragala, I. L.; Marks, T. J. *Organometallics* **2006**, *25*, 5533.  
 (53) Motta, A.; Lanza, G.; Fragala, I. L.; Marks, T. J. *Organometallics* **2004**, *23*, 4097.  
 (54) Tobisch, S. *Chem.–Eur. J.* **2005**, *11*, 6372.  
 (55) Tobisch, S. *J. Am. Chem. Soc.* **2005**, *127*, 11979.  
 (56) Tobisch, S. *Chem.–Eur. J.* **2006**, *12*, 2520.  
 (57) Senn, H. M.; Blochl, P. E.; Togni, A. *J. Am. Chem. Soc.* **2000**, *122*, 4098.  
 (58) Dobado, J. A.; Molina, J. M.; Uggla, R.; Sundberg, M. R. *Inorg. Chem.* **2000**, *39*, 2831.  
 (59) Froese, R. D. J.; Musaev, D. G.; Morokuma, K. *J. Am. Chem. Soc.* **1998**, *120*, 1581.  
 (60) Michalak, A.; Ziegler, T. *Organometallics* **2000**, *19*, 1850.  
 (61) Backvall, J. E.; Bjorkman, E. E.; Pettersson, L.; Siegbahn, P. *J. Am. Chem. Soc.* **1984**, *106*, 4369.  
 (62) Siegbahn, P. E. M.; Stromberg, S.; Zetterberg, K. *Organometallics* **1996**, *15*, 5542.  
 (63) Niu, S.; Zoric, S.; Bayse, C. A.; Strout, D. L.; Hall, M. B. *Organometallics* **1998**, *17*, 5139.  
 (64) Albert, K.; Gisdakis, P.; Rosch, N. *Organometallics* **1998**, *17*, 1608.  
 (65) von Schenck, H.; Stromberg, S.; Zetterberg, K.; Ludwig, M.; Akermark, B.; Svensson, M. *Organometallics* **2001**, *20*, 2813.  
 (66) All calculations were carried out with the Gaussian 03 program: Frisch, M. J.; *Gaussian 03*, revision C.02; Gaussian Inc.: Wallingford, CT, 2004. See the Supporting Information for the full reference.

- (67) Pitcock, W. H., Jr.; Lord, R. L.; Baik, M.-H. *J. Am. Chem. Soc.* **2008**, *130*, 5821.  
 (68) Yu, Z.-X.; Cheong, P. H.-Y.; Liu, P.; Legault, C. Y.; Wender, P. A.; Houk, K. N. *J. Am. Chem. Soc.* **2008**, *130*, 2378.  
 (69) Wiedemann, S. H.; Lewis, J. C.; Ellman, J. A.; Bergman, R. G. *J. Am. Chem. Soc.* **2006**, *128*, 2452.  
 (70) Fristrup, P.; Kreis, M.; Palmelund, A.; Norrby, P.-O.; Madsen, R. *J. Am. Chem. Soc.* **2008**, *130*, 5206.  
 (71) Shen, Z.; Dornan, P. K.; Khan, H. A.; Woo, T. K.; Dong, V. M. *J. Am. Chem. Soc.* **2009**, *131*, 1077.  
 (72) Huang, J.; Haar, C. M.; Nolan, S. P.; Marshall, W. J.; Moloy, K. G. *J. Am. Chem. Soc.* **1998**, *120*, 7806.  
 (73) Selent, D.; Scharfenberg-Pfeiffer, D.; Reck, G.; Taube, R. *J. Organomet. Chem.* **1991**, *415*, 417.

Scheme 2 adopt structure **B** in which the centroid of the ethylene C=C bond lies out of the plane of the rhodium and the other three ligands. In the idealized structure **A**, the M–C bond distances are equal, and the angle between the centroid of the C–C bond of the alkene, the metal, and the ligand that is trans to the alkene is 180°. The specific Rh–C bond distances and P–Rh–centroid angles for our optimized structure are as follows: (PMe<sub>3</sub>)<sub>2</sub>Rh( $\eta^2$ -C<sub>2</sub>H<sub>4</sub>)(CH<sub>3</sub>), Rh–C = 2.18 and 2.21 Å, P–Rh–centroid angle = 156°; (PMe<sub>3</sub>)<sub>2</sub>Rh( $\eta^2$ -C<sub>2</sub>H<sub>4</sub>)(NH<sub>2</sub>), Rh–C = 2.17 and 2.18 Å, P–Rh–centroid angle = 152°; (PMe<sub>3</sub>)<sub>2</sub>Rh( $\eta^2$ -C<sub>2</sub>H<sub>4</sub>)(OH), Rh–C = 2.17 and 2.18 Å, P–Rh–centroid angle = 163°.

We propose that structure **B** may be observed when a d<sup>8</sup> metal center is electron rich and can participate in strong backbonding interactions with the coordinated alkene. In these cases, the resonance structure of a five-coordinate, d<sup>6</sup> metallacyclopropane dominates. A square-based pyramidal structure, which would resemble the metallacyclopropane form of structure **B**, is typically more stable for a five-coordinate d<sup>6</sup> metal center than is a trigonal-bipyramidal structure, which would resemble the metallacyclopropane form of structure **A**. We propose that structure **A** may be observed when the transition metal is less electron rich and, thus, participates in weaker backbonding interactions with the coordinated alkene (as is the case with cationic Pd(II) or Pt(II) complexes).

The computed relative enthalpies and free energies of the ethylene complexes (PMe<sub>3</sub>)<sub>2</sub>Rh( $\eta^2$ -C<sub>2</sub>H<sub>4</sub>)(X) (X = CH<sub>3</sub>, NH<sub>2</sub>, OH) are given in Scheme 2. The computed free energies of activation for C–X bond formation within these complexes by migratory insertion decrease in the order C (**1a-TS**) > O (**1b-TS**) > N (**1c-TS**). These barriers are consistent with the faster rates determined experimentally for reactions that occur by insertion of alkenes into the Rh–N and –O bonds of amido<sup>45</sup> and alkoxo<sup>46</sup> complexes than into the Rh–C bond of an analogous alkyl complex.<sup>45,46</sup>

The relative energies of the initial products of migratory insertion follow a different trend (X = OH (**1c-P**) > X = CH<sub>3</sub> (**1a-P**) > X = NH<sub>2</sub> (**1b-P**)) than those of the transition states. In each case, the transition state for migratory insertion leads to an initial product that has some type of Rh–X interaction. The migratory insertion of **1a-R** (X = CH<sub>3</sub>) leads to a complex (**1a-P**) in which one of the C–H bonds of the terminal methyl group participates in an agostic interaction with the rhodium center. This initial complex containing a  $\gamma$ -agostic interaction is likely to rearrange to a complex containing a  $\beta$ -agostic structure. The structure containing a  $\beta$ -agostic interaction is computed to be more stable than that containing a  $\gamma$ -agostic interaction by 6.7 kcal/mol in free energy (7.3 kcal/mol in enthalpy) and more stable in free energy than the starting  $\eta^2$ -alkene complex (**1a-R**) by 8.7 kcal/mol. However, such a rearrangement of the initial structure of the insertion product does not affect the energetics of the insertion because it is a separate process that occurs after the insertion event.

In contrast to the initial product of the migratory insertion of **1a**, the initial products of C–N and C–O bond formation arising from **1b** and **1c** are computed to have metallacyclic structures that retain a Rh–N or Rh–O bond. In these transformations, the X-type<sup>74</sup> Rh–N and Rh–O bonds of the starting complexes become L-type<sup>74</sup> (dative) Rh–N and Rh–O dative bonds in the products. As expected, this Rh–N dative bond in the azametallacycle of **1b-P** is stronger than the Rh–O dative bond

in the oxacycle of **1c-P**, and the product from insertion of ethylene into the amide (**1b-P**) is 15.5 kcal/mol more stable relative to the respective reactant than is the product from insertion of ethylene into the metal–hydroxo complex (**1c-P**). Insertion of ethylene into the rhodium–hydroxo complex is endothermic, presumably because of the strong Rh–O bond in the reactant and the relatively weak Rh–O interaction between the alcohol oxygen and the neutral, low-valent rhodium in the oxacyclic product.

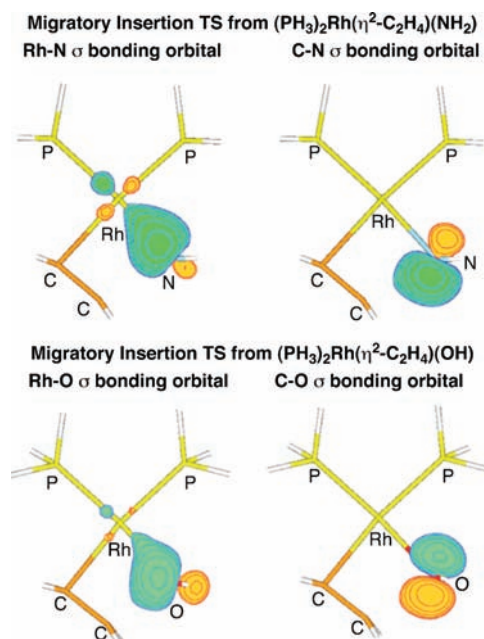
To provide an estimate of the magnitude of the Rh–X interaction in the product, we optimized a structural isomer of each product (**1a-P**, **1b-P**, and **1c-P**) in which the P–Rh–C–C dihedral angles were frozen at 0° and 180° so that the CH<sub>2</sub>CH<sub>2</sub>X group is rotated in such a way that neither a C–H bond of the original methyl group nor the X atom of the original amido or hydroxo group can interact with the rhodium center. These three-coordinate,  $\kappa^1$ -CH<sub>2</sub>CH<sub>2</sub>X structures (**2a-c**) were computed to be less stable than those possessing Rh–X dative or C–H agostic interactions with the rhodium center (**1a-P**, **1b-P**, and **1c-P**) by differences in energy that increase in the order Rh–C < Rh–O < Rh–N. Because these three-coordinate complexes contain fixed dihedral angles and are not true minima on the potential-energy surface, we compared the computed electronic energies ( $\Delta E$ ) of the metallacyclic and acyclic structures, rather than the  $\Delta H$  or  $\Delta G$  values. These two forms of the alkyl complex (**1a-P** and **2a**) are nearly isoenergetic ( $\Delta E$  = 1.6 kcal/mol), but the electronic energy of the oxacycle (**1c-P**) is lower than that of the acyclic isomer (**2c**) by 12.7 kcal/mol, and the electronic energy of the azacycle (**1b-P**) is lower than that of the acyclic isomer (**2b**) by 19.4 kcal/mol.

Although the C–C and C–X bonds in the products are likely to differ, based on known C–C, C–N, and C–O bond strengths in alkanes, amines, and alcohols,<sup>75</sup> the trends in thermodynamics for the insertion process to form the metallacyclic structures appear to follow the expected strengths of the dative bonds in the product versus the strengths of the covalent bonds in the reactants. Bryndza, Bercaw, and co-workers concluded that the homolytic bond enthalpies of Pt–X bonds decrease in the order Pt–O > Pt–C  $\gg$  Pt–N.<sup>76</sup> In the products from alkene insertion, the M–X bond strengths most likely follow the order M–N > M–O  $\gg$  M–C. The M–N and M–O dative bonds to the metal are calculated to be stronger than the C–H agostic interaction, and the M–N bond to the neutral amine nitrogen atom is calculated to be stronger than the M–O bond to the neutral alcohol oxygen atom. Thus, insertion of ethylene into the Rh–NH<sub>2</sub> bond cleaves the weakest covalent bond in the three reactants and forms the metallacycle containing the strongest dative bond, leading to the most exothermic reaction of this series. Insertion of ethylene into the Rh–OH bond cleaves the strongest covalent bond of the three reactants and forms the metallacycle containing a dative bond of intermediate strength. This process is, therefore, less favored thermodynamically than insertion into the Rh–NH<sub>2</sub> bond and is calculated to be endothermic. Insertion of ethylene into the Rh–CH<sub>3</sub> bond cleaves a covalent bond of intermediate strength and forms a metallacycle containing the weakest dative interaction, making this process intermediate in

(75) Luo, Y.-R. *Handbook of Bond Dissociation Energies in Organic Compounds*; CRC Press: Boca Raton, FL, 2003.

(76) Bryndza, H. E.; Fong, L. K.; Paciello, R. A.; Tam, W.; Bercaw, J. E. *J. Am. Chem. Soc.* **1987**, *109*, 1444.

(74) Green, M. L. H. *J. Organomet. Chem.* **1995**, *500*, 127.



**Figure 2.** Natural localized molecular orbitals for the C–X and Rh–X  $\sigma$  bonds of transition-state structures from  $(\text{PH}_3)_2\text{Rh}(\eta^2\text{-C}_2\text{H}_4)(\text{NH}_2)$  and  $(\text{PH}_3)_2\text{Rh}(\eta^2\text{-C}_2\text{H}_4)(\text{OH})$ . Orbitals are rendered at an isodensity value of 0.10.

thermodynamic driving force. The insertion process is calculated to be nearly thermoneutral.

**Bonding Analysis for the Small Model Complexes  $(\text{PH}_3)_2\text{Rh}(\eta^2\text{-C}_2\text{H}_4)(\text{X})$  ( $\text{X} = \text{CH}_3, \text{NH}_2, \text{OH}$ ).** The wave functions derived from these calculations of the transition-state structures for migratory insertion and immediate products of C–X bond formation were examined by computation and visualization of the natural localized molecular orbitals (NLMOs) derived from natural bond orbital (NBO) analysis<sup>77</sup> (Figure 2), and the molecular electron densities derived from these computations were examined using Bader's AIM analysis.<sup>78</sup> The NBO and AIM analysis are two independent methods to examine the electronic structure of a molecule. AIM analysis examines the topology of the total electron density, while NBO analysis localizes the individual occupied molecular orbitals. The NBO analysis transforms the occupied delocalized canonical molecular orbitals into a set of localized molecular orbitals by maximizing the sum of squares of the centroids of occupied molecular orbitals while preserving the orthonormality of the orbitals. Ideally, this transformation yields orbitals that consist of lone pairs of electrons on atoms and electron pairs in  $\sigma$ -,  $\pi$ -, and  $\delta$ -bonding orbitals between pairs of atoms. The AIM theory examines the chemical bonding of a molecule by examining the topology of the molecular electron density. In the context of AIM theory, two atoms are chemically bonded if their atomic volumes share a common interatomic surface and there is a critical point on this surface where the gradient of the electron density is zero. In other words, in AIM theory, the presence of a bond critical point (BCP) between two atoms indicates a chemical bond between these atoms and the absence of a BCP between the two atoms indicates the absence of a chemical bond between these atoms. These two types of computations were conducted on smaller models of the methyl, amido, and hydroxo

complexes in which  $\text{PH}_3$  ligands were used in place of the  $\text{PEt}_3$  ligands of the experimental system to allow for the use of the large, all-electron basis sets required for these methods. The computed enthalpies and free energies, transition states for migratory insertion, and initial products of migratory insertion for reactions of the  $\text{PH}_3$  complexes are given in Scheme SI-I of the Supporting Information. The trend in free energy barriers for the migratory insertion of ethylene into the Rh–X bonds and the trend in free energies for the migratory insertion of ethylene into the Rh–X bonds were the same as those calculated for analogous reactions of the  $\text{PMe}_3$  complexes.

**Atoms-in-Molecules (AIM) Analysis of Bonding for Migratory Insertion of Ethylene Into Rh–X Bonds of  $(\text{PH}_3)_2\text{Rh}(\eta^2\text{-C}_2\text{H}_4)(\text{X})$  ( $\text{X} = \text{CH}_3, \text{NH}_2, \text{OH}$ ).** Bader's atoms-in-molecules (AIM) method<sup>78</sup> helped reveal the differences in bonding between the starting  $\eta^2$ -alkene complexes, the transition states for migratory insertion, and the products of migratory insertion of ethylene into the three types of rhodium complexes. Plots of the computed bond critical points in the reactant, immediate products, and transition-state structures for migratory insertion are given in Figures S1–S9 of the Supporting Information. For each reactant, the AIM analysis indicates the presence of bonds between the Rh center and both carbon atoms of the olefin and a bond between the Rh center and the carbon or heteroatom of the X group. Similarly, for all three transition-state structures, the AIM analysis indicates the presence of bonds between the Rh center and both carbon atoms of the alkene, a bond between the Rh center and the carbon or heteroatom of the X group, and a bond between one carbon of the alkene and the carbon or heteroatom of the X group. In contrast, this method indicates significant differences in the bonding of the immediate products formed from migratory insertion of the alkene into the Rh–X bond. There is no bond between the Rh center and the methyl carbon of the product from migratory insertion into the methyl complex, whereas the immediate product of migratory insertion of bound ethylene into the metal–amido and –hydroxo bonds retains a Rh–N or Rh–O bond.

A more quantitative analysis of AIM results provides insight into the origin of the experimentally observed lower barriers for migratory insertion of ethylene into the Rh–N and Rh–O bonds versus the Rh–C bond. The computed electron density at the bond critical point between two atoms has been shown in previous work to assess the bond order between those two atoms.<sup>58,78–94</sup> We compared the computed electron densities at the BCP's of the Rh–C, C–X, and Rh–X bonds in the reactant, transition-state structures, and initial products to determine the changes in bonding that occur during C–X bond

(79) Angyan, J. G.; Loos, M.; Mayer, I. *J. Phys. Chem.* **1994**, *98*, 5244.

(80) Bader, R. F. W.; Chang, C. *J. Phys. Chem.* **1989**, *93*, 5095.

(81) Chesnut, D. B. *J. Phys. Chem. A* **2003**, *107*, 4307.

(82) Chesnut, D. B.; Quin, L. D. *J. Comput. Chem.* **2004**, *25*, 734.

(83) Chopra, D.; Zhurov, V. V.; Zhurova, E. A.; Pinkerton, A. A. *J. Org. Chem.* **2009**, *74*, 2389.

(84) Cioslowski, J.; Mixon, S. T. *J. Am. Chem. Soc.* **1991**, *113*, 4142.

(85) DuPre, D. B.; Wong, J. L. *J. Phys. Chem. A* **2005**, *109*, 7606.

(86) Firme, C. L.; Antunes, O. A. C.; Esteves, P. M. *J. Phys. Chem. A* **2007**, *111*, 11904.

(87) Fradera, X.; Sola, M. *J. Comput. Chem.* **2002**, *23*, 1347.

(88) Love, I. *J. Phys. Chem. A* **2006**, *110*, 10507.

(89) Love, I. *J. Phys. Chem. A* **2009**, *113*, 2640.

(90) Matta, C. F.; Arabi, A. A.; Keith, T. A. *J. Phys. Chem. A* **2007**, *111*, 8864.

(91) Mayer, I. *J. Comput. Chem.* **2007**, *28*, 204.

(92) Murgich, J.; Franco, H. J. *J. Phys. Chem. A* **2009**, *113*, 5205.

(93) Pakiari, A. H.; Jamshidi, Z. *J. Phys. Chem. A* **2008**, *112*, 7969.

(94) Werstiuk, N. H.; Wang, Y.-G. *J. Phys. Chem. A* **2001**, *105*, 11515.

(77) Foster, J. P.; Weinhold, F. *J. Am. Chem. Soc.* **1980**, *102*, 7211.

(78) Bader, R. F. *Atoms in Molecules: A Quantum Theory*; Oxford University Press: Oxford, U.K., 1990.

formation. Comparison of the computed electron density at the BCP of the Rh–X bond of the reactant to the computed electron density at the BCP of the transition-state structure reveals the changes in bond order between the reactants and transition states. Similarly, comparison of the computed electron density at the BCP of the forming C–X bond of the transition-state structure to the computed electron density at the BCP of the fully formed C–X bond of the product yields the bond order of the transition-state structure relative to the bond order in the product.

The Rh–N and Rh–O bond orders in the transition states for migratory insertion of the  $(\text{PH}_3)_2\text{Rh}(\eta^2\text{-C}_2\text{H}_4)(\text{NH}_2)$  and  $(\text{PH}_3)_2\text{Rh}(\eta^2\text{-C}_2\text{H}_4)(\text{OH})$  complexes are much higher than the Rh–C bond order in the transition state for migratory insertion of the  $(\text{PH}_3)_2\text{Rh}(\eta^2\text{-C}_2\text{H}_4)(\text{CH}_3)$  complex. This analysis estimates that the Rh–C bond is 49% broken in the transition state for C–C formation and that the new C–C bond is 34% formed. In contrast, this analysis estimates that the Rh–N bond is only 23% broken in the transition state for C–N formation, while the C–N bond is 23% formed; the Rh–O bond is only 24% broken in the transition state for C–O formation, while the C–O bond is 29% formed. In other words, the smaller extent of cleavage of the Rh–N or Rh–O bond to form the transition states for migratory insertion is largely compensated by formation of the new C–N and C–O bonds, whereas the larger amount of cleavage of the C–C bond to form the transition state for migratory insertion is less balanced by C–C bond formation. Thus, the larger degree of Rh–X bonding retained in the transition states for insertion into Rh–N and Rh–O bonds explains the computed and experimentally observed lower barriers for insertion into the Rh–N and Rh–O bonds of the amido and hydroxo complexes, even though the transition state for insertion into the Rh–C bond reflects slightly more C–X bond making than the transition states for C–N and C–O formation.

**Natural Localized Molecular Orbital (NLMO) Analysis of  $(\text{PH}_3)_2\text{Rh}(\eta^2\text{-C}_2\text{H}_4)(\text{X})$  ( $\text{X} = \text{CH}_3, \text{NH}_2, \text{OH}$ ).** Analysis of the natural localized molecular orbitals in the transition-state structures for migratory insertion from  $(\text{PH}_3)_2\text{Rh}(\eta^2\text{-C}_2\text{H}_4)(\text{X})$  ( $\text{X} = \text{NH}_2, \text{OH}$ ) provide further support for the presence of Rh–X bonding in both of these species. Plots of the natural localized molecular orbitals for the Rh–N, Rh–O, C–N, and C–O  $\sigma$ -bonding orbitals in these transition states are given in Figure 2. In contrast to the conclusion from AIM analysis, the NLMO's of the transition state for migratory insertion involving the methyl group in  $(\text{PH}_3)_2\text{Rh}(\eta^2\text{-C}_2\text{H}_4)(\text{CH}_3)$  indicate the presence of the newly forming C–C bond but not a remaining Rh–C  $\sigma$  bond to the carbon of the original methyl group. These results suggest that the Rh–C bond is fully broken when the new C–C bond is forming during migration of the methyl group to the coordinated alkene. However, like the conclusion from AIM analysis, the NLMO's of the transition state for reaction of the amido and hydroxo complexes  $(\text{PH}_3)_2\text{Rh}(\eta^2\text{-C}_2\text{H}_4)(\text{X})$  imply the presence of significant Rh–N and Rh–O during formation of the C–N and C–O bonds.

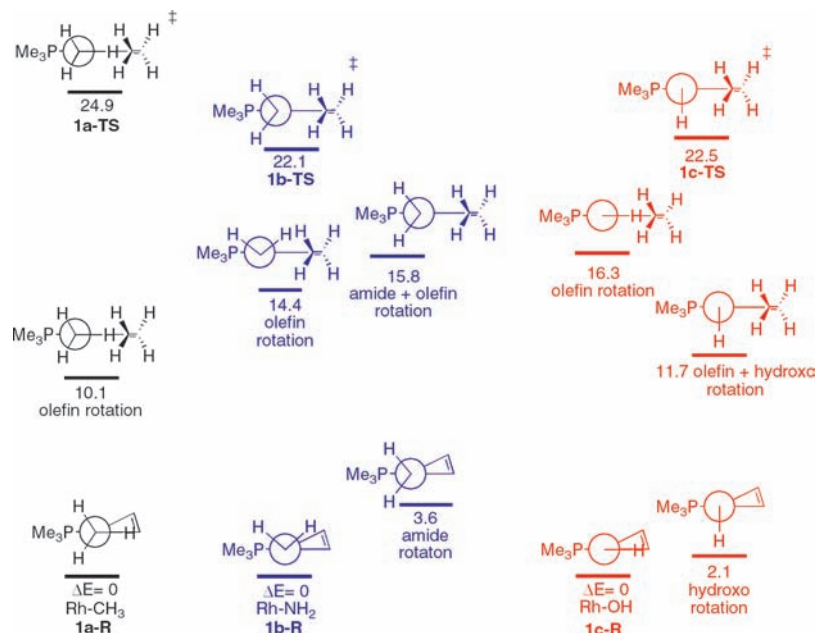
A comparison of the optimized structures of the reactant complexes and the transition states for migratory insertion of alkenes further supports the assertion that there is much more Rh–C bond breaking in the transition state for reaction of the Rh–CH<sub>3</sub> complex than Rh–N or Rh–O bond breaking in the transition state for reaction of the Rh–NH<sub>2</sub> and Rh–OH complexes. The change in Rh–C bond distance between the ground and transition state is larger than the changes in Rh–N or Rh–O bond distances between the analogous two structures.

The Rh–C bond to the methyl group in  $(\text{PMe}_3)_2\text{Rh}(\eta^2\text{-C}_2\text{H}_4)(\text{CH}_3)$  was calculated to be 2.18 Å, while the Rh–C distance in the transition-state structure was found to be 2.36 Å. The Rh–heteroatom bond distances in  $(\text{PMe}_3)_2\text{Rh}(\eta^2\text{-C}_2\text{H}_4)(\text{X})$  ( $\text{X} = \text{NH}_2, \text{OH}$ ) were calculated to be 2.03 and 2.05 Å, respectively, for  $\text{X} = \text{NH}_2$  and  $\text{OH}$ , while the Rh–X distances in the transition-state structures were calculated to be 2.12 and 2.15 Å for  $\text{X} = \text{NH}_2$  and  $\text{OH}$ .

Although the degree of Rh–C bonding in the transition state for migratory insertion of  $(\text{PH}_3)_2\text{Rh}(\eta^2\text{-C}_2\text{H}_4)(\text{CH}_3)$  was different when analyzed by NLMO's and AIM theory, the trends in the extent of bonding deduced from these methods are consistent with each other. Both NLMO and AIM analysis indicate that a much higher degree of Rh–N and Rh–O bonding is retained in the transition states and immediate products of migratory insertion of  $(\text{PH}_3)_2\text{Rh}(\eta^2\text{-C}_2\text{H}_4)(\text{X})$  ( $\text{X} = \text{NH}_2, \text{OH}$ ) than in the transition states and immediate products of migratory insertion of  $(\text{PH}_3)_2\text{Rh}(\eta^2\text{-C}_2\text{H}_4)(\text{CH}_3)$ .

**Dissection of the Reorganization Energy Required To Achieve the Transition States for Migratory Insertion of Ethylene Into the Rh–X Bonds of  $(\text{PMe}_3)_2\text{Rh}(\eta^2\text{-C}_2\text{H}_4)(\text{X})$  ( $\text{X} = \text{CH}_3, \text{NH}_2, \text{OH}$ ).** The origins of the relative energies of the transition states for migratory insertion into the Rh–C, Rh–N, and Rh–O bonds were further revealed by calculating the energies of structures in which the alkene and hydrogen atoms of the amido or alkoxo ligand have been rotated to adopt the orientations of the transition-state structure. This analysis provides a sense of the relative energetic contributions of structural reorganization, versus the combination of bond formation and bond cleavage, to the relative energies of the transition states for migratory insertion into the three types of complexes. To adopt the transition-state structures, the alkene ligand, as well as the amide and alkoxo ligands, must each rotate by roughly 90°. To determine the energies of the different conformers, the orientations of the alkene ligand, the orientations of the hydrogen atoms of the amido or hydroxo ligands, or both, were held constant by freezing the P–Rh–C–C dihedral angle, the P–Rh–X–H dihedral angle, or both, and allowing the other structural parameters to optimize freely. Because of this restraint, these optimized structures, like the structures of the acyclic forms of the insertion products, are not true minima on the potential-energy surface, and therefore, this analysis of the reorganization to achieve the transition-state structure is based on a comparison of electronic energies ( $\Delta E$ ) rather than  $\Delta H$  and  $\Delta G$  values. The  $\Delta E$  values for these transition states are close but not identical to the  $\Delta H$  values (and therefore  $\Delta G$  values due to the intramolecularity of the insertion process) that correspond to the transition states in Scheme 1. The results of this analysis are shown as the ladder of energies in Figure 3. The complexes containing different conformers of the alkene and of the amido or hydroxo ligands are represented in this figure as Newman projections viewed along the Rh–X bond.

The conformations of the  $(\text{PMe}_3)_2\text{Rh}(\eta^2\text{-C}_2\text{H}_4)(\text{CH}_3)$ ,  $(\text{PMe}_3)_2\text{Rh}(\eta^2\text{-C}_2\text{H}_4)(\text{NH}_2)$ , and  $(\text{PMe}_3)_2\text{Rh}(\eta^2\text{-C}_2\text{H}_4)(\text{OH})$  complexes in which the alkene lies in the square plane, as it does in the transition-state structure for migratory insertion, was obtained by constraining the P–Rh–C–C dihedral angles to the values that are obtained from the fully optimized transition-state structures and allowing the other atoms to optimize freely. This structure of the methyl complex was calculated to be 10.1 kcal/mol less stable in energy than that of the starting complex, whereas these structures for the amido and hydroxo complexes



**Figure 3.** Energy ladders corresponding to alkene rotation, CH<sub>3</sub>, NH<sub>2</sub>, or OH rotation, and the combination of these two geometric changes that precede the transition state. Values are computed electronic energies ( $\Delta E$ ) and given in kcal/mol relative to the reactant.

were calculated to be 14.4 and 16.3 kcal/mol less stable in energy than the reactant complexes.<sup>95–100</sup>

The orientation of the hydrogen atom(s) attached to the NH<sub>2</sub> and OH groups (and therefore heteroatom electron lone pairs) are computed to be different in the reactant complexes and transition-state structures for migratory insertion. In the ground-state reactant complex **1b-R**, both hydrogen atoms of the NH<sub>2</sub> group lie on the same side of the square plane, and the lone pair lies perpendicular to the square plane. However, in the transition-state structure for migratory insertion into the Rh–N bond (**1b-TS**), the hydrogen atoms lie above and below the square plane and the lone pair lies in the square plane pointing toward the alkene. In the ground-state reactant complex **1c-R**, the hydrogen atom of the OH group lies in the square plane pointed toward the alkene, while in the transition-state structure for migratory insertion into the Rh–O bond (**1c-TS**), the hydrogen atom lies perpendicular to the square plane and one of the lone pairs lies in the square plane pointing toward the alkene.

The structures in which the NH<sub>2</sub> and OH ligands are oriented as they are in the transition-state structures have been computed by constraining the P–Rh–N–H and P–Rh–O–H dihedral angles to the values that are contained in the fully optimized transition-state structures. The optimized structure in which the electron pair of the nitrogen atom of (PMe<sub>3</sub>)<sub>2</sub>Rh( $\eta^2$ -C<sub>2</sub>H<sub>4</sub>)(NH<sub>2</sub>) is oriented toward the alkene in the square plane was calculated to be 3.6 kcal/mol less stable in energy than the ground-state structure in which the electron pair lies perpendicular to the

square plane. The optimized structure in which the hydrogen atom of the OH ligand lies in the plane is only 2.1 kcal/mol less stable in energy than the ground-state structure.

The structures in which both the amido or hydroxo ligand and the alkene ligand are oriented as they are in the transition-state structures have been computed by constraining the P–Rh–C–C and P–Rh–X–H (X = N, O) dihedral angles to the values that are contained in the fully optimized transition-state structures. The optimized structure in which both the NH<sub>2</sub> hydrogen atoms and the alkene carbon atoms are oriented as they are in the transition-state structure was calculated to be 15.8 kcal/mol less stable than the ground state. The optimized structure in which both the OH hydrogen atom and the alkene carbon atoms are oriented as they are in the transition-state structure was calculated to be 11.7 kcal/mol less stable than the ground state. Thus, the differences in energies between the transition states and the (PMe<sub>3</sub>)<sub>2</sub>Rh( $\eta^2$ -C<sub>2</sub>H<sub>4</sub>)(X) (X = CH<sub>3</sub>, NH<sub>2</sub>, OH) conformers containing the atoms oriented in the geometry of the transition state through simple bond rotations are 14.8 kcal/mol for the methyl complex, 10.8 kcal/mol for the hydroxo complex, and only 6.3 kcal/mol for the amido complex. Although conformational changes certainly occur simultaneously with bond formation and bond cleavage, this analysis of the contribution of conformational changes and the combination of bond formation and cleavage shows that the combination of bond formation and cleavage during insertion of the alkene into the amido ligand occurs with little barrier, that this combination of events occurs during migratory insertion into the hydroxo ligand with a higher but still relatively low barrier, and that this combination of events occurs during insertion into the methyl complex with the highest barrier.

**Relative Rates and Regioselectivity of Migratory Insertion of Propene into Rh–X Bonds of (PMe<sub>3</sub>)<sub>2</sub>Rh( $\eta^2$ -C<sub>2</sub>H<sub>4</sub>)(X) (X = CH<sub>3</sub>, NH<sub>2</sub>, OH).** The migratory insertion of propene into a metal–alkyl, –amido, and –alkoxo complex can occur by 1,2-insertion to form a primary alkyl intermediate or by 2,1-insertion to form a secondary alkyl intermediate. In some cases, the insertion of an alkene into a metal–carbon bond occurs to form

(95) These values are consistent with measurable barriers for rotations of coordinated olefins in square-planar Rh(I) complexes. See refs 96–100.

(96) Aresta, M.; Quaranta, E.; Albinati, A. *Organometallics* **2002**, *12*, 2032.

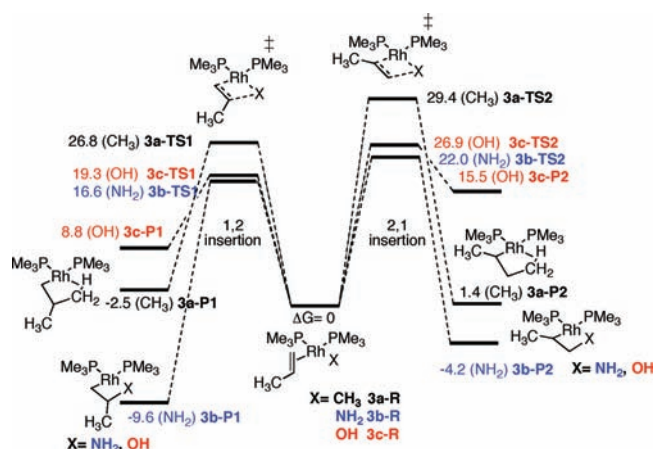
(97) Thaler, E. G.; Caulton, K. G. *Organometallics* **2002**, *9*, 1871.

(98) Arthurs, M.; Al-Daffaee, H. K.; Haslop, J.; Kubal, G.; Pearson, M. D.; Thatcher, P.; Curzon, E. *Dalton Trans.* **1987**, 2615.

(99) Arthurs, M.; Bickerton, J. C.; Kirkley, M.; Palin, J.; Piper, C. J. *Organomet. Chem.* **1992**, *429*, 245.

(100) Arthurs, M. A.; Nelson, S. M. *J. Coord. Chem.* **1983**, *13*, 29.

Scheme 3



the primary alkyl intermediate; in other cases, it forms the secondary alkyl intermediate; and in yet other cases it occurs to form nearly equal mixtures of the two isomers.<sup>48,101</sup> In all cases of catalytic and stoichiometric reactions proposed to occur by insertions of unactivated alkenes into metal alkoxo or amido complexes, products that would result from 1,2-insertion to form the primary alkyl intermediate have been observed.<sup>29,46,49</sup> Thus, we conducted calculations to determine the relative energetics for migratory insertion of the simplest substituted alkene, propene, into the rhodium–methyl, –amido, and –alkoxo complexes to form products of 1,2- and 2,1-insertion. These calculations provide a sense of the barrier for the experimentally unobserved 2,1-insertion of an alkene into an amido or alkoxo ligand and insight into the origins of the regioselectivity.

Scheme 3 shows the starting structures, immediate products, and transition states for 1,2- and 2,1-insertions into the PMe<sub>3</sub>-ligated rhodium–methyl, –amido, and –hydroxo complexes.<sup>102</sup> The 1,2-migratory insertion of the coordinated propene in (PMe<sub>3</sub>)<sub>2</sub>Rh( $\eta^2$ -CH<sub>2</sub>CHMe)(CH<sub>3</sub>) is calculated to occur with a free energy of activation ( $\Delta G^\ddagger$ ) and free energy ( $\Delta G$ ) that are similar to those for migratory insertion of the coordinated ethylene in (PMe<sub>3</sub>)<sub>2</sub>Rh( $\eta^2$ -C<sub>2</sub>H<sub>4</sub>)(CH<sub>3</sub>). The 1,2-migratory insertions of propene in the complexes (PMe<sub>3</sub>)<sub>2</sub>Rh( $\eta^2$ -CH<sub>2</sub>CHMe)(NH<sub>2</sub>) and (PMe<sub>3</sub>)<sub>2</sub>Rh( $\eta^2$ -CH<sub>2</sub>CHMe)(OH) are calculated to occur with free energy barriers that are significantly lower than those calculated for migratory insertion of ethylene in the complexes (PMe<sub>3</sub>)<sub>2</sub>Rh( $\eta^2$ -C<sub>2</sub>H<sub>4</sub>)(NH<sub>2</sub>) and (PMe<sub>3</sub>)<sub>2</sub>Rh( $\eta^2$ -C<sub>2</sub>H<sub>4</sub>)(OH). The immediate products are calculated to be slightly more stable than those derived from the insertion of ethylene.

Most striking is the substantial increase in the difference in free energy barriers ( $\Delta\Delta G^\ddagger$ ) for 1,2- and 2,1-migratory insertion of propene (TS1 versus TS2 in Scheme 3) with an increase in

the electronegativity of the metal-bound atom of the methyl, amido, and hydroxo ligands. The computed barriers for 1,2- and 2,1-migratory insertion of propene into the rhodium–carbon bond of (PMe<sub>3</sub>)<sub>2</sub>Rh( $\eta^2$ -CH<sub>2</sub>CHMe)(CH<sub>3</sub>) (3a-TS1 and 3a-TS2) are similar to each other; the barrier for 1,2-migratory insertion in this complex is only slightly lower (2.6 kcal/mol) than that for 2,1-migratory insertion. In contrast, the computed free energy barriers for 1,2-insertion of the coordinated propene in (PMe<sub>3</sub>)<sub>2</sub>-Rh( $\eta^2$ -CH<sub>2</sub>CHMe)(NH<sub>2</sub>) and (PMe<sub>3</sub>)<sub>2</sub>Rh( $\eta^2$ -CH<sub>2</sub>CHMe)(OH) are much lower than those for 2,1-insertion. The computed  $\Delta\Delta G^\ddagger$  for reaction of the amido complex was 5.4 kcal/mol (3b-TS1 versus 3b-TS2), and the computed  $\Delta\Delta G^\ddagger$  for reaction of the hydroxo complex was 7.6 kcal/mol (3c-TS1 versus 3c-TS2). These computed values for  $\Delta\Delta G^\ddagger$  are consistent with the experimental observation of a slight preference for 1,2-insertion over 2,1-insertion of alkenes into late transition-metal–alkyl bonds and the exclusive formation of products derived from 1,2-insertion into late transition-metal–amide and –alkoxide bonds, noted in the Introduction.

These differences in barriers for formation of 1,2- versus 2,1-migratory insertion parallel the differences in energies of the initial products formed from these two reactions. The initial products from 1,2-insertion into the Rh–CH<sub>3</sub>, Rh–NH<sub>2</sub>, and Rh–OH bonds of the three complexes are 3.9, 5.4, and 6.7 kcal/mol more stable, respectively, than the initial products from 2,1-insertion into the Rh–C, Rh–N, and Rh–O bonds of the same complexes.

We attribute the preference for formation of products from 1,2- versus 2,1-insertion to two factors. First, the product from 1,2-insertion is favored because of the greater stability of a primary versus secondary alkyl group in most transition-metal complexes.<sup>103</sup> The origin of this difference in energy has been attributed to both steric and electronic effects.<sup>103</sup> In addition to the obvious reduced steric interaction, the partial negative charge on a metal-bound carbon atom of an alkyl ligand is thought to be more stable at a primary position than at a secondary position. Although these arguments account for the preferential formation of 1,2- over 2,1-insertion products, the marked increase in  $\Delta\Delta G^\ddagger$  with increasing electronegativity of the atom bound to the metal in the starting material must result from a second electronic effect. We propose that the increasing magnitude of  $\Delta\Delta G^\ddagger$  with increasing electronegativity results from the increasing ionic character of the C–X bond and accompanying increasing positive charge on the carbon bound to the methyl, amino, or hydroxyl group. The more substituted this carbon, the greater the stabilization of this increasing positive charge.

The effect of the electronegativity of the atom bound to the metal on the magnitude of  $\Delta\Delta G^\ddagger$  for formation of primary versus secondary alkyl intermediates parallels the effect of electronegativity on the magnitude of the difference in energy of linear versus branched alkanes, amines, and alcohols.<sup>104–107</sup> This electronic effect can be appreciated by comparing linear versus branched alkanes, amine, and alcohols containing four heavy atoms. Experimental and computed values for the difference in heats of formation ( $\Delta\Delta H_f^\circ$ ) of linear and branched butanes, propylamines, and propyl alcohols are shown in Table 1. To determine the computed relative heats of formation, a

(101) Svejda, S. A.; Johnson, L. K.; Brookhart, M. *J. Am. Chem. Soc.* **1999**, *121*, 10634.

(102) For the starting olefin complexes (PMe<sub>3</sub>)<sub>2</sub>Rh( $\eta^2$ -CH<sub>2</sub>CHMe)(X) (X = CH<sub>3</sub>, NH<sub>2</sub>, or OH), the rhodium center can be bound to either face of the propene ligand, leading to complexes in which the methyl group of propene is oriented toward or away from the X ligand. Both possible isomers of these starting complexes were examined at the DZP/B3LYP level. For the complex in which X = CH<sub>3</sub>, the methyl group of the propene ligand is oriented away from the rhodium-bound methyl group in the most stable isomer. For the complex in which X = NH or OH, the methyl group of the propene ligand is oriented away from the rhodium-bound X group in the most stable isomer. The relative energies in Scheme 3 are reported in the lowest energy form of the propene complexes in each case. The higher energy olefin complexes lie 1.3–2.0 kcal/mol higher in enthalpy and 1.2–1.9 kcal/mol higher in free energy.

(103) Harvey, J. N. *Organometallics* **2001**, *20*, 4887.

(104) Gronert, S. *J. Org. Chem.* **2006**, *71*, 7045.


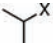
(105) Exner, K.; Schleyer, P. v. R. *J. Phys. Chem. A* **2001**, *105*, 3407.

(106) Wodrich, M. D.; Wannere, C. S.; Mo, Y.; Jarowski, P. D.; Houk, K. N.; Schleyer, P. v. R. *Chem.–Eur. J.* **2007**, *13*, 7731.



(107) Ingold, K. U.; DiLabio, G. A. *Org. Lett.* **2006**, *8*, 5923.



**Table 1.** Computed and Experimental Relative Heats of Formation of Alkanes, Amines, and Alcohols

|                   |  |                        |  |                        |
|-------------------|---|------------------------|---|------------------------|
|                   | $\Delta H(\text{calc})$   | $\Delta H(\text{exp})$ | $\Delta H(\text{calc})$   | $\Delta H(\text{exp})$ |
| X=CH <sub>3</sub> | 0.85  | (1.03)                 | 0.00  | (0.00)                 |
| X=NH <sub>2</sub> | 2.66  | (3.28)                 | 0.00  | (0.00)                 |
| X=OH              | 3.97  | (3.85)                 | 0.00  | (0.00)                 |

|      |  |                        |  |                        |
|------|---|------------------------|---|------------------------|
|      | $\Delta H(\text{calc})$   | $\Delta H(\text{exp})$ | $\Delta H(\text{calc})$   | $\Delta H(\text{exp})$ |
| X=NH | 2.04  | (-)                    | 0.00  | (-)                    |
| X=O  | 3.29  | (-)                    | 0.00  | (-)                    |

number of rotational isomers were computed for each positional isomer, and the lowest energy rotational isomers were compared. The values in Table 1 show that the branched alkane isobutane is more stable enthalpically than *n*-butane by 1.03 kcal/mol (computed  $\Delta H = 0.85$  kcal/mol), that isopropylamine is more stable enthalpically than *n*-propylamine by a larger 3.28 kcal/mol (computed  $\Delta H = 2.66$  kcal/mol), and that isopropanol is more stable than *n*-propanol by an even larger 3.85 kcal/mol (computed  $\Delta H = 3.97$  kcal/mol). Thus, the magnitudes of the  $\Delta\Delta H$  values for alkanes, amines, and alcohols increases with increasing electronegativity of the atom bound to the branch point of the structure.

We also evaluated the relative stabilities of methyl-substituted oxetanes and azetidines to determine if the same trend is observed for cyclic compounds. Experimental heats of formation are unavailable for these compounds; therefore, computed relative enthalpies are given. The same trend that was observed for the linear molecules was observed for these four-membered ring heterocycles. The structures in which the methyl group is  $\alpha$  to the heteroatom are more stable than the isomers in which the methyl group is located  $\beta$  to the heteroatom. Specifically, 1-methyl azetidine is calculated to be more stable enthalpically than 2-methyl azetidine by 2.0 kcal/mol, whereas 1-methyl oxetane is calculated to be more stable enthalpically than 2-methyl oxetane by 3.3 kcal/mol.

## Summary

We examined the effects of the X group on the structures and energies of intermediates and transition states for migratory insertion of alkenes into the M–X bonds of methyl, amido, and hydroxo complexes of rhodium possessing the formula  $(\text{PMe}_3)_2\text{Rh}(\eta^2\text{-alkene})(\text{X})$  (X = CH<sub>3</sub>, NH<sub>2</sub>, OH). The following conclusions were drawn from our studies.

(1) The calculated free energy barriers for migratory insertion of the alkene in the most stable conformers of the starting complexes  $(\text{PMe}_3)_2\text{Rh}(\eta^2\text{-alkene})(\text{X})$  (X = CH<sub>3</sub>, NH<sub>2</sub>, OH) follow the trend Rh–NH<sub>2</sub> < Rh–OH  $\ll$  Rh–CH<sub>3</sub>.

(2) We attribute the lower computed free energy barrier for migratory insertion of ethylene into the metal–alkoxo and –amido bonds, relative to migratory insertion into the metal–alkyl bonds, to the presence of an M–X dative bond in the transition state and immediate insertion product. Thus, the original X-type M–N or M–O bond in the starting complex is transformed into an L-type M–N or M–O dative bond during the insertion process. Because the M–X bond (X = NH<sub>2</sub>, OH) is transformed into a different type of metal–ligand bond during the insertion process, rather than broken, a higher rhodium–ligand bond order is present in the transition state for insertion into the Rh–O

and Rh–N bonds than is present in the transition state for insertion into the Rh–C bond.

(3) Computations of the natural localized molecular orbitals of the transition states and products for migratory insertion reactions of  $(\text{PH}_3)_2\text{Rh}(\eta^2\text{-C}_2\text{H}_4)(\text{X})$  (X = CH<sub>3</sub>, NH<sub>2</sub>, OH) and analysis of the bond orders of these species using Bader's atoms-in-molecules method support the presence of much stronger M–X interactions in the transition-state structure and the immediate products of migratory insertion when X = NH<sub>2</sub> and OH than when X = CH<sub>3</sub>.

(4) Substantial energy is required for the starting complexes to adopt the conformations of the transition-state structures, and the relative transition-state energies for migratory insertion into the Rh–NH<sub>2</sub> and Rh–OH bonds can be rationalized by the differences in these reorganization energies. We propose that the larger reorganization energy for reaction of the Rh–NH<sub>2</sub> complex than for reaction of the Rh–OH complex causes the slightly higher barrier for migratory insertion into the Rh–OH complex, despite formation of the more stable product from insertion into the Rh–NH<sub>2</sub> bond.

(5) The barriers to migratory insertion from the species in which the C<sub>2</sub>H<sub>4</sub> and hydrogen atoms of the X ligands have the orientation of the transition-state structure follow the trend M–NH<sub>2</sub> < M–OH < M–CH<sub>3</sub>. A very low barrier to C–N bond formation was found by these calculations. These barriers were calculated to be 9.4 kcal/mol for insertion into the Rh–CH<sub>3</sub> bond, 7.5 kcal/mol for insertion into the Rh–O bond, and only 2.6 kcal/mol for insertion into the Rh–NH<sub>2</sub> bond.

(6) The differences in barriers for 1,2-migratory insertion versus 2,1-migratory insertion of propene into the metal–hydroxo, –amido, and –methyl complexes were calculated. The computed  $\Delta\Delta G^\ddagger$  for 1,2- versus 2,1-insertion of the alkene into the metal–alkoxo bond was found to be greater than that for the two types of insertions into the metal–amido bond, which was found to be greater than that for the two types of insertions into the metal–alkyl bond. Because this trend follows the order of electronegativities of the atoms, the origin of this effect appears to result from the polarity of the bonds in the transition state. We propose that the transition state containing the more polar C–X bond is more stabilized by the alkyl substituent than is the transition state containing the less polar C–X bond. This proposal is consistent with the known relative stabilities of linear versus branched alcohols, amines, and alkanes. The differences in energies between the branched and linear isomers of these small molecules increases with increasing electronegativity.

Although the energies calculated in this work are specific to the rhodium system, the general conclusions about the changes in bonding from reactants to transition state for migratory insertion by the three types of complexes in this work should pertain to migratory insertions of other late transition-metal–alkyl, –amido, and –alkoxo complexes. Such insertions have been deduced from experimental mechanistic studies to occur with palladium complexes, as noted in the Introduction, although an absence of precise structural information on the alkoxo and amido complexes that undergo the migratory insertion process precludes correlations of energies of computed systems with experimental systems. Moreover, most of the proposed intermediates in Wacker processes are charged and, therefore, more difficult to model. Nevertheless, the conclusions deduced from the studies reported here should apply to many additional low-valent, late transition-metal complexes, particularly those with square-planar geometries, and our calculated barriers for the migratory insertions of alkenes into metal–alkyl,

–amido, and –hydroxo bonds are consistent with the few pieces of experimental data on the relative reactivity of these classes of compounds toward alkenes noted in the Introduction.

Although experimental evidence for insertions of alkenes into late transition-metal–amido and –alkoxo bonds exists, the number of examples of reactions that occur by this pathway is smaller than the number that occur by insertions of alkenes into metal–carbon bonds. Thus, if the barriers for insertions of bound olefins into metal–amido and metal–alkoxo bonds are similar to or lower than those for insertions of bound alkenes into metal–alkyl bonds, then why have alkene insertions into metal–nitrogen and metal–oxygen bonds seldom been observed? We suggest that the small number of examples results from the need for an open coordination site *cis* to the alkoxide or amide. Monomeric complexes containing an open coordination site that is sufficiently available for binding the alkene often forms stable dimeric species containing bridging alkoxides or amides. Thus, complexes that favor binding of an alkene over

dimerization are required for insertion to occur. Although the features that lead to this selectivity are not known at this time, it is clear that complexes possessing such reactive, monomeric forms can be accessed because both catalytic reactions and defined stoichiometric reactions have been shown to occur by migratory insertions of alkenes into metal–nitrogen and metal–oxygen bonds.

**Acknowledgment.** We thank the DOE for support of this work and Prof. Michael Hall (Texas A&M University) for helpful discussions.

**Supporting Information Available:** Computational details, computed enthalpies and free energies, plots of the bond critical points and ring critical points derived from the AIM analysis, and full citation for the Gaussian 03 program (ref 66). This material is available free of charge via the Internet at <http://pubs.acs.org>.

JA901945B